Collective magnetic excitations of Ho^{3+} ions in grain-aligned $HoBa_2Cu_3O_x$ (x=7, 6.2)

1995 J. Phys.: Condens. Matter 7 4215

(http://iopscience.iop.org/0953-8984/7/22/005)

J. Phys.: Condens. Matter 7 (1995) 4215–4226. Printed in the UK

Collective magnetic excitations of Ho^{3+} ions in grain-aligned $HoBa_2Cu_3O_x$ ($x = 7, 6.2$)

F Fauth†, U Staub†, M Guillaume†, J Mesot†, A Furrer†, P Dosanjh‡, H Zhou‡ and P Vorderwisch§

† Laboratory for Neutron Scattering, ETH Zürich and Paul Scherrer Institut, CH-5232 Villigen PSI, Switzerland

‡ University of British Columbia, Department of Physics, Vancouver BC, Canada

§ Berlin Neutron Scattering Centre, Hahn-Meitner-Institut, D-14109 Berlin, Germany

Abstract. Inelastic neutron scattering (INS) has been used to study the magnetic excitations of Ho^{3+} ions in grain-aligned samples of $HoBa_2Cu_3O_x$ in both orthorhombic ($x \approx 7$) and tetragonal ($x \approx 6.2$) phases. The magnetic excitations associated with the lowest ground state crystalline electric field transition exhibit dispersion in the (a, b) plane but remain constant in energy along the c axis. The data are analysed in the random-phase approximation in terms of a generalized Heisenberg model including anisotropies in the coupling of the spin operators.

1. Introduction

In nearly all high-T_c superconductors $RBa_2Cu_3O_7$ (R = rare earth) long-range magnetic order of the R^{3+} ion sublattice appears at very low temperatures: three-dimensional antiferromagnetic structures with different propagation vectors were determined by means of neutron diffraction [1]. The oxygen content in the systems $RBa_2Cu_3O_x$ plays an important role for the superconducting properties as well as for the magnetic interactions: a transition from three- to two-dimensional magnetic structures is observed when oxygen is removed from $ErBa_2Cu_3O_7$ and $NdBa_2Cu_3O_7$ [2, 3]. In order to understand the interplay of superconductivity and magnetism, it is necessary to get information on both the electronic ground state of the R^{3+} ions and the coupling mechanism between the R^{3+} ions. Whereas it is relatively easy to determine the ground state wavefunctions in the systems $RBa_2Cu_3O_x$, particularly through neutron spectroscopic investigations of the crystalline electric field (CEF) interaction, there is still a lack of information concerning both the nature and the size of the magnetic interaction. Several mechanisms leading to two- or three-dimensional spin structures are generally proposed for these systems: Ruderman–Kittel–Kasuya–Yosida (RKKY), dipolar or superexchange interactions. ^{155}Gd Mössbauer spectroscopy data obtained for $GdBa_2Cu_3O_7$ revealed a small number of conduction electrons at Gd^{3+} sites implying only very weak RKKY interactions [4]. Misra and Felsteiner [5] calculated the expected low-temperature ordered states for various $RBa_2Cu_3O_7$ compounds based on dipolar interactions alone, but their prediction in the case R = Ho disagrees with recent neutron diffraction data [6]. Furthermore, as it is the case for $GdBa_2Cu_3O_x$ [7] and $RBa_2Cu_3O_7$ with R = Nd, Dy, Er [8], calculations based on dipolar interactions alone generally result in Néel temperatures which are lower than the observed ordering temperatures implying that exchange interaction has to be considered in the magnetic coupling between R^{3+} ions.

Qualitative information on the coupling of the R^{3+} ions in the systems $RBa_2Cu_3O_7$ has been obtained from magnetization and low- temperature specific heat measurements which

0953-8984/95/224215+12$19.50

indicate large anisotropies of the magnetic interaction in the (a, b) plane [9]. However, a more detailed insight into the coupling mechanism is possible from a study of the spin dynamics. Measurements of the collective magnetic excitations which inherently contain information on both the nature and the size of the magnetic coupling between the R^{3+} ions turn out to be the most direct way to characterize the magnetic interaction. The inelastic neutron scattering (INS) technique is particularly suited for this kind of study which is usually performed on single crystals. Because of the absence of sufficiently large and perfect crystals of $RBa_2Cu_3O_x$ we have performed our experiments on grain-aligned samples. This technique has already been applied in a preliminary study of $HoBa_2Cu_3O_7$ [10], but here we present INS data obtained under improved experimental conditions for grain-aligned samples of $HoBa_2Cu_3O_x$ in both orthorhombic ($x \approx 7$) and tetragonal ($x \approx 6.2$) phases. The reason for the choice of this particular rare earth element lies essentially in the well known CEF level scheme of $HoBa_2Cu_3O_x$ which is characterized by a series of low-lying states which can be sufficiently resolved within the small range of energy dispersion anticipated for these systems [11, 12].

2. Experimental details and results

Polycrystalline single-phase starting material of $HoBa_2Cu_3O_7$ of weight 15 g was prepared by a standard sintering procedure and oxygenated to reach a maximum oxygen content close to seven. In $HoBa_2Cu_3O_7$ the crystalline electric field acting on the rare earth ion induces a strong anisotropy in the single-ion susceptibility $\chi_0^\alpha(\omega)$ ($\alpha = x, y, z$): the z axis is the easy axis of magnetization at high temperatures [11]. It follows from this property that the application of an external magnetic field results in an alignment of the grains along the z axis, whereas the x and y axes remain randomly oriented. To align the powder, 7 ml heptane and 0.8 g sarcosyl-O was first added to the sample. The mixture was milled for 50 minutes and quickly poured into three Teflon moulds. The samples were then placed into a magnetic field of 5.24 T at 500 °C for 7 days. The resulting oriented samples had a grain size of less than 1 μm. At this point the samples were very soft and hard to handle. Once the pellets were removed from the Teflon holder they were put into a tube furnace set at 205 °C for 2 hours and then at 400 °C for another 2 hours. This allowed us to burn off any organic materials that remained from the sarcosyl-O. Finally the pellets were taken to 920 °C for 5 hours, after which time they were annealed in pure O_2 for 2 days at 400 °C. The tetragonal phase $HoBa_2Cu_3O_{6.2}$ was obtained from the grain-aligned $HoBa_2Cu_3O_7$ sample by a temperature-controlled oxygen desorption–absorption procedure. The quality of the alignment was characterized by neutron diffraction: the rocking curves measured for various $(00l)$ reflections turned out to be of Gaussian shape with HWHM $\approx 11°$ (see figure 1, upper part). We also performed 2θ scans of the (001) reflection for values of ω ranging from 0° to 90°, and the resulting integrated intensities are shown in the lower part of figure 1. For perfect grain alignment the integrated intensities should vanish at large values of ω. However, we do observe some minor Bragg scattering at large ω values which means that our samples still contain unaligned powder. From figure 1 we determine the fraction of unaligned powder to be about 15%.

The INS experiments were performed at the Hahn-Meitner-Institut, Berlin, with use of the high-resolution triple-axis spectrometer V2 installed at a cold-neutron guide. The spectrometer was equipped with a vertically bent pyrolitic graphite monochromator to gain intensity and a pyrolitic planar graphite analyser, both with (002) scattering planes. Collimators of 60′ were used between the monochromator and the sample and before and after the analyser. The energy of the scattered neutrons was kept fixed at 3.5 meV

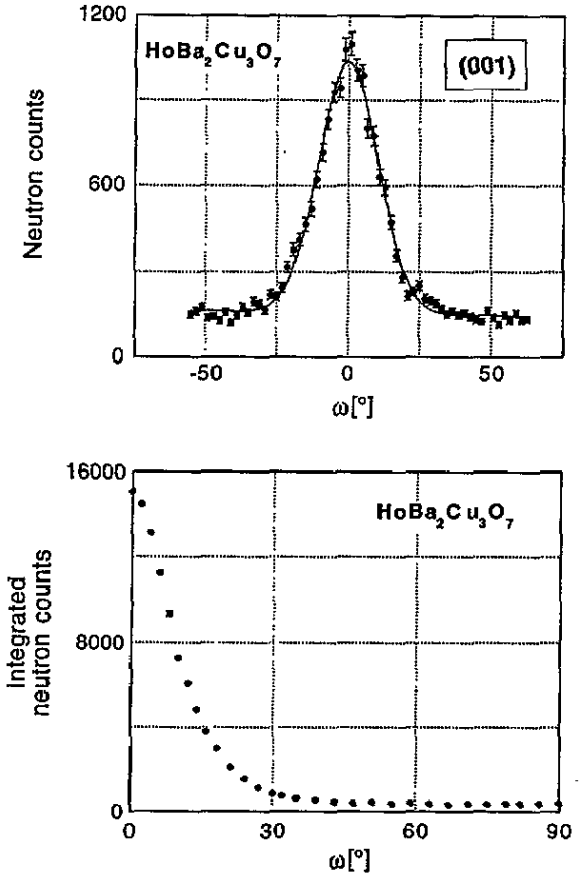

Figure 1. Rocking curve of the (001) reflection in $HoBa_2Cu_3O_7$ measured with use of a double-axis spectrometer at PSI (upper part) and integrated intensities of 2θ scans as function of ω (lower part). The line is a Gaussian fit to the data.

for $HoBa_2Cu_3O_7$ and 3.08 meV for $HoBa_2Cu_3O_{6.2}$, resulting in an energy resolution of 0.09 meV and 0.07 meV at $\Delta E = 0$, respectively. The samples were oriented with the [001] axis in the scattering plane and mounted in an 'orange ILL-type' helium cryostat to achieve the temperature $T \approx 1.5$ K which is far above the ordering temperature of Ho^{3+} moments in $HoBa_2Cu_3O_x$ (long-range antiferromagnetism was found below $T_N = 190$ mK for $x = 7$, whereas no magnetic superlattice reflections were detected for $x = 6.3$) [6]. A cooled beryllium filter was inserted between monochromator and sample to eliminate higher-order contamination. Scans with constant scattering vector $Q = 2\pi(x/a, y/b, z/c)$ were performed throughout the experiments. Due to the random orientation of the samples in the (a, b) plane, it was impossible to distinguish between the components Q_x and Q_y lying perpendicular to the z axis, therefore the actual scattering vector was $Q = 2\pi(x'/a, z/c)$ with $x' = \sqrt{x^2 + y^2}$ (assuming $a = b$).

For both orthorhombic and tetragonal phases of $HoBa_2Cu_3O_x$ we covered a large region of reciprocal space in the (x', z) plane, and for all Q the first ground state CEF excitation was examined in detail. In $HoBa_2Cu_3O_7$, some Q have been extended to include also the third ground state CEF excitation $\Gamma_3 \rightarrow \Gamma_1$ of energy 3.8 meV [11]. In $HoBa_2Cu_3O_7$ the CEF transition $\Gamma_3 \rightarrow \Gamma_4$ of energy $\Delta \approx 0.5$ meV [11] shows up as a well resolved

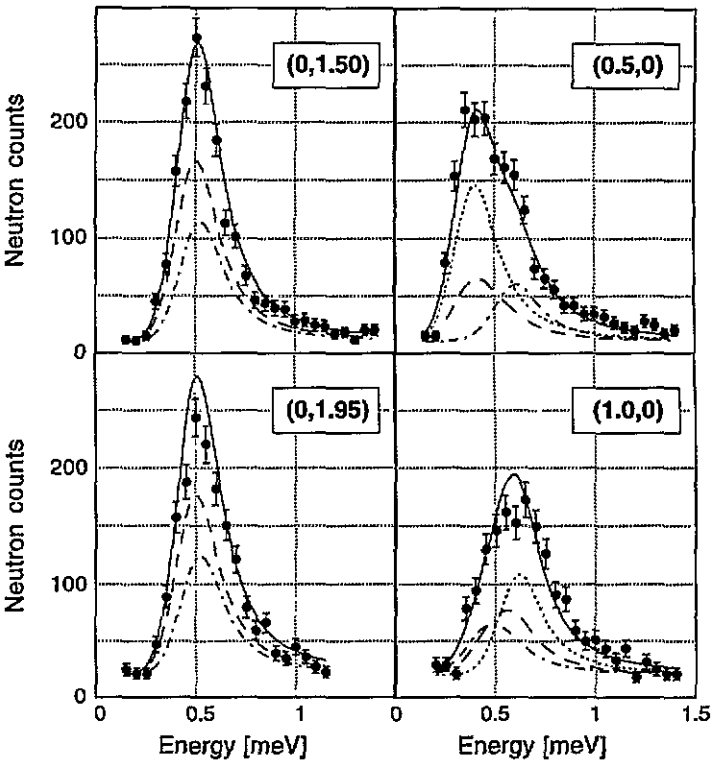

Figure 2. Normalized and form-factor-corrected energy spectra of neutrons scattered from grain-aligned $HoBa_2Cu_3O_7$ at 1.5 K for Q parallel and perpendicular to the c axis. The full lines correspond to the calculated excitation spectra as explained in the text. The broken, dash–dotted and dotted lines represent x, y and z polarizations, respectively.

inelastic line and exhibits dispersion in energy as exemplified in figure 2. The peak shape is broad and asymmetric for Q perpendicular to the z axis, whereas for Q involving a zero x' component we observed narrow but still asymmetric lines. The energy of maximum peak intensity of this excitation varies typically between 0.4 and 0.6 meV when following Q along the x' axis and remains constant upon variation of Q along the z axis. Further illustrative energy spectra of neutrons scattered from grain-aligned $HoBa_2Cu_3O_7$ are shown in figure 3. For $HoBa_2Cu_3O_{6.2}$ the ground state CEF transition $\Gamma_3 \rightarrow \Gamma_5$ of energy $\Delta \approx 1.1$ meV [12] exhibits a considerably reduced dispersion in energy, but the line shape still appears asymmetric (figure 4).

3. Data analysis

3.1. Theoretical background

In our experiments on grain-aligned $HoBa_2Cu_3O_x$ the data are analysed in terms of a phenomenological spin Hamiltonian of the form

$$H = \sum_i H_{\mathrm{CEF}}(i) - \frac{1}{2}\sum_{ij} J_{ij}^{\perp}(J_i^x J_j^x + J_i^y J_j^y) + J_{ij}^{\parallel} J_i^z J_j^z. \qquad (1)$$

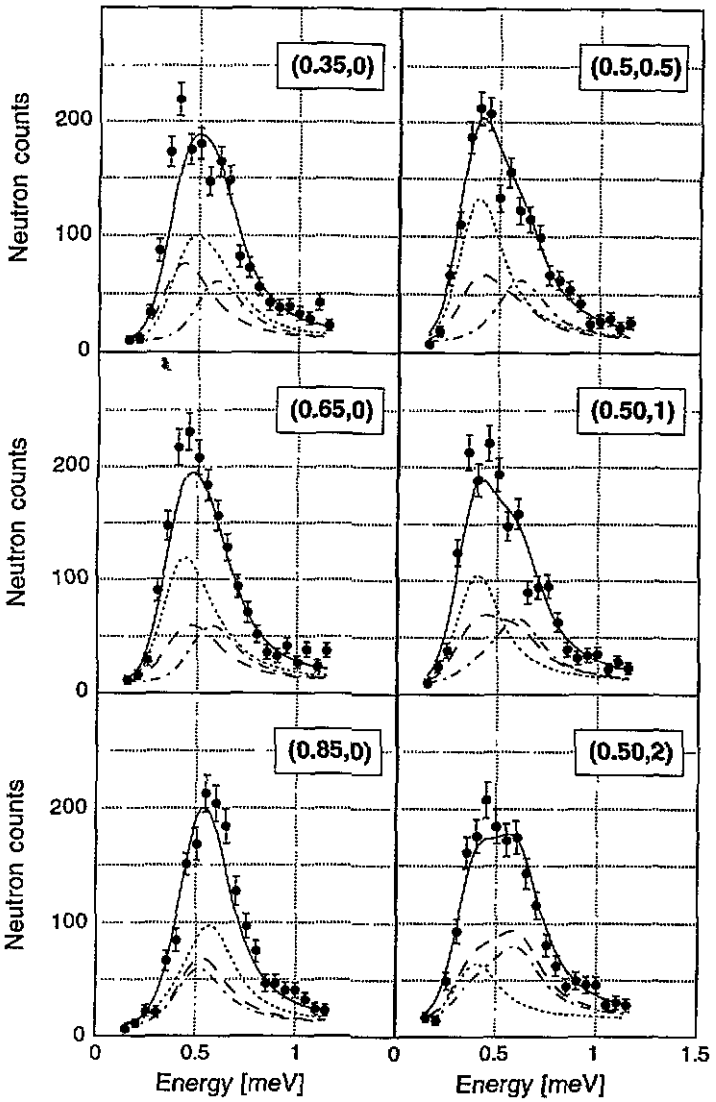

Figure 3. Normalized and form-factor-corrected energy spectra of neutrons scattered from grain-aligned $HoBa_2Cu_3O_7$ at 1.5 K for scattering vectors along the $(x', 0)$ and $(0.5, z)$ directions. The lines are as in figure 2.

The single-ion term $H_{CEF}(i)$ describes the crystalline electric field (CEF) interaction at the Ho^{3+} sites which was entirely determined by means of INS experiments performed on polycrystalline $HoBa_2Cu_3O_x$ [11, 12]. The two-ion term reduces to the well known Heisenberg, Ising and XY models for $J_{ij}^{\perp} = J_{ij}^{\parallel}$, $J_{ij}^{\perp} = 0$ and $J_{ij}^{\parallel} = 0$, respectively. For $J_{ij}^{\perp} \neq J_{ij}^{\parallel} \neq 0$ we have a general anisotropic model. In the random-phase approximation, the magnetic excitations are determined by the poles of the dynamic magnetic susceptibility [13, 14]:

$$\chi^{\alpha}(Q,\omega) = \frac{\chi_0^{\alpha}(\omega)}{1 - J^{\alpha}(Q)\chi_0^{\alpha}(\omega)} \qquad \alpha = (x, y, z) \tag{2}$$

where $J^\alpha(Q)$ ($x, y = \perp,\ z = \parallel$) is the Fourier transform of the exchange coupling and $\chi_0^\alpha(\omega)$ the single-ion susceptibility. The integrated intensities $I^\alpha(Q)$ of the excitations are proportional to the residues of the corresponding poles. Inelastic neutron scattering experiments yield the magnetic excitations or the inelastic part of the dynamic magnetic susceptibility. The cross section is [15]

$$\frac{\partial^2\sigma}{\partial\Omega\,\partial\omega} \sim F^2(Q)\sum_\alpha\left(1-\frac{Q_\alpha^2}{Q^2}\right)\Im\chi^\alpha(Q,\omega) \tag{3}$$

where $F(Q)$ is the magnetic form factor. Because of the polarization factor $[1-(Q_\alpha/Q)^2]$ neutrons can only couple to spin fluctuations perpendicular to the scattering vector Q, which allows us to distinguish the different polarizations of the magnetic excitations.

In principle, the dispersion curves of the magnetic excitations and the intensities have to be calculated numerically. However, the energy of the first ground state CEF transition in $HoBa_2Cu_3O_x$ is sufficiently small compared to the energies of the other CEF transitions that we can assume an effective two-level system for which the following simple expressions for energies $\omega^\alpha(Q)$ and integrated intensities $I^\alpha(Q)$ result [16]:

$$\omega^\alpha(Q) = \Delta\sqrt{1-\frac{2M_\alpha^2 J^\alpha(Q)}{\Delta}\tanh\left(\frac{\Delta}{2k_BT}\right)} \tag{4a}$$

$$I^\alpha(Q) = M_\alpha^2\frac{\Delta}{\omega^\alpha(Q)}. \tag{4b}$$

Here, Δ corresponds to the energy of the CEF transition from the ground state $|0\rangle$ to the excited state $|1\rangle$, and $M_\alpha = \langle 1|J^\alpha|0\rangle$ ($\alpha = x, y, z$) is the dipole transition matrix element between these two states. Both M_α and Δ are known from previous CEF measurements on powders [11, 12].

For the calculation of $J^\alpha(Q)$ we take into account the exchange parameters J_a^α, J_b^α and J_c^α coupling the central Ho^{3+} ion with the nearest-neighbour Ho^{3+} ions at the positions $\pm a$, $\pm b$ and $\pm c$ along the x, y, and z directions, respectively. From the absence of dispersion along the z axis in $HoBa_2Cu_3O_7$ and $HoBa_2Cu_3O_{6.2}$ (figures 2, 4) we immediately conclude that $J_c^\alpha \approx 0$ as actually expected from the large separation of the Ho^{3+} ions along that axis. Information about J_a^α and J_b^α is more difficult to obtain because of the random orientation of the x and y axes in our samples. Therefore, the magnetic excitation spectra cannot be analysed directly according to (4*a*) and (4*b*), but a superposition procedure has to be performed in the (x, y) plane. In this procedure, we calculate the magnetic excitation energies $\omega^\alpha(Q)$ and the corresponding intensities $I^\alpha(Q)$ for various directions of Q in the (x, y) plane by varying the direction cosines systematically, obtaining a histogram-like energy and intensity distribution. In order to compare the model calculations and the observed spectra, the energy and intensity distribution is then convoluted with a line shape function which describes both the instrumental resolution as well as an asymmetric tail appearing on the high-energy side. The asymmetric line shape becomes evident from figures 2 and 4. It clearly does not result from our superposition procedure since it is also present in the spectra with $Q = (0, z)$ where no averaging has to be performed. In fact, this asymmetric line shape of the CEF transition in $HoBa_2Cu_3O_x$ was already observed in earlier work [11, 12, 17], and different models based on fluctuating magnetic or electric fields at the R^{3+} sites were proposed in [17] to explain this effect.

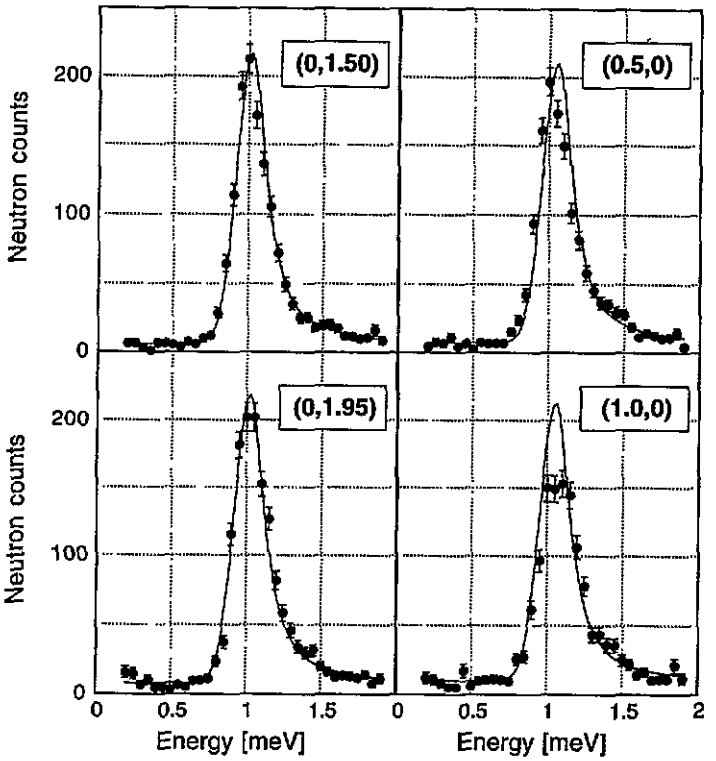

Figure 4. Normalized and form-factor-corrected energy spectra of neutrons scattered from grain-aligned $HoBa_2Cu_3O_{6.2}$ at 1.5 K for Q parallel and perpendicular to the c axis. The lines are as in figure 2.

3.2. $HoBa_2Cu_3O_7$

Twenty-one measured energy spectra of the CEF ground state transition $\Gamma_3 \rightarrow \Gamma_4$ in $HoBa_2Cu_3O_7$ were least squares fitted to our model. In a first step, parameters concerning the convoluted line shape function (a half-width parameter for the Gaussian type of both the intrinsic broadening of the CEF line and the instrumental resolution as well as an anisotropic line shape factor) were deduced from the spectra with $x' = 0$ where no superposition procedure is necessary. Then all the spectra were simultaneously fitted to our model with the following disposable parameters: an overall scaling factor, the CEF transition energy Δ, the three CEF dipole transition matrix elements M_x, M_y, M_z with the condition $M_x^2 + M_y^2 + M_z^2 = 27$ for $HoBa_2Cu_3O_7$ [11], and the magnetic coupling parameters $J_a^{\perp}$, $J_a^{\parallel}$, $J_b^{\perp}$ and $J_b^{\parallel}$. The resulting parameters for grain-aligned $HoBa_2Cu_3O_7$ are given in Table 1 for both the anisotropic and isotropic models. Calculated and measured spectra are shown in figures 2 and 3. From the goodness of the fit we conclude that the Heisenberg model is inferior to the model with anisotropic magnetic coupling parameters.

Due to the random orientation of the x and y axes in our grain-aligned sample another solution is possible by interchanging the parameters J_a^{α} and J_b^{α}, but our choice of ferromagnetic and antiferromagnetic coupling along the a and b axes, respectively, is consistent with the low-temperature neutron diffraction study of the magnetic ordering in $HoBa_2Cu_3O_7$ [6]. There is a good agreement between our CEF transition energy Δ and previous results obtained from CEF measurements on powders [11]. The fitted

exchange parameters also correspond well to those determined from the dimer excitations in $Y_{0.9}Ho_{0.1}Ba_2Cu_3O_7$ where $J_a = -J_b = 2.6 \pm 0.3$ meV [17]. From our data we calculate the molecular field parameters $\lambda^\alpha = J^\alpha(q_0) = 2(J_a^\alpha - J_b^\alpha - J_c^\alpha)$, where $q_0 = [0, \frac{1}{2}, \frac{1}{2}]$ is the ordering wave vector [6], to be $\lambda^\perp = 5.6 \pm 0.2$ μeV and $\lambda^\parallel = 6.9 \pm 0.3$ μeV, which are in good agreement with $\lambda^x = 5.6$ μeV derived from the zero-field magnetization [6].

Table 1. Refined parameters for both anisotropic and isotropic magnetic coupling in $HoBa_2Cu_3O_7$.

Anisotropic model	Isotropic model
$J_a^\perp = 3.2 \pm 0.7$ μeV	
	$J_a = 2.2 \pm 1.1$ μeV
$J_a^\parallel = 0 \pm 0.2$ μeV	
$J_b^\perp = -2.4 \pm 0.8$ μeV	
	$J_b = -2.4 \pm 1.2$ μeV
$J_b^\parallel = -6.9 \pm 1.6$ μeV	
$\Delta = 0.52 \pm 0.02$ meV	$\Delta = 0.52 \pm 0.02$ meV
$M_x^2 = 11.4 \pm 2.4$	$M_z^2 = 14.0 \pm 5.0$
$M_y^2 = M_z^2 = 7.8 \pm 1.2$	$M_y^2 = M_z^2 = 6.5 \pm 2.5$
$\chi^2 = 2.4$	$\chi^2 = 3.3$

Table 2. Refined parameters for both anisotropic and isotropic magnetic coupling in $HoBa_2Cu_3O_{6.2}$.

Anisotropic model	Isotropic model
$J^\perp = 0.7 \pm 0.6$ μeV	
	$J = 0.6 \pm 0.4$ μeV
$J^{zz} = -2.2 \pm 4.5$ μeV	
$\Delta = 1.05 \pm 0.02$ meV	$\Delta = 1.05 \pm 0.01$ meV
$M_\perp^2 = 23.1 \pm 3.8$	$M_\perp^2 = 23.2 \pm 1.4$
$M_z^2 = 8.9 \pm 1.9$	$M_z^2 = 8.8 \pm 0.7$
$\chi^2 = 2.4$	$\chi^2 = 2.6$

In order to check the reliability of the derived magnetic coupling parameters we have calculated three measured spectra corresponding to the $\Gamma_3 \rightarrow \Gamma_1$ ground state CEF transition of energy $\Delta \approx 3.8$ meV [11] on the basis of the anisotropic magnetic coupling parameters listed in table 1; the only varied parameters were an overall scale factor, the CEF transition energy Δ, and the three CEF transition matrix elements M_x, M_y, M_z with the condition $M_x^2 + M_y^2 + M_z^2 = 5$ [11]. The resulting transition energy, $\Delta = 3.92 \pm 0.03$ meV, corresponds well to previous measurements on powders, and the transition matrix elements are $M_x^2 = M_y^2 = 0.6 \pm 0.2$ and $M_z^2 = 3.8 \pm 0.4$. The good agreement between the observed and the calculated energy spectra (figure 5) proves the reliability of the magnetic coupling parameters obtained from the analysis of the $\Gamma_3 \rightarrow \Gamma_4$ CEF transition.

3.3. $HoBa_2Cu_3O_{6.2}$

In the tetragonal phase $HoBa_2Cu_3O_{6.2}$ we studied in detail the lowest CEF ground state transition $\Gamma_3 \rightarrow \Gamma_5$ of energy $\Delta = 1.1$ meV [12]. Here, the dispersion effects involved are

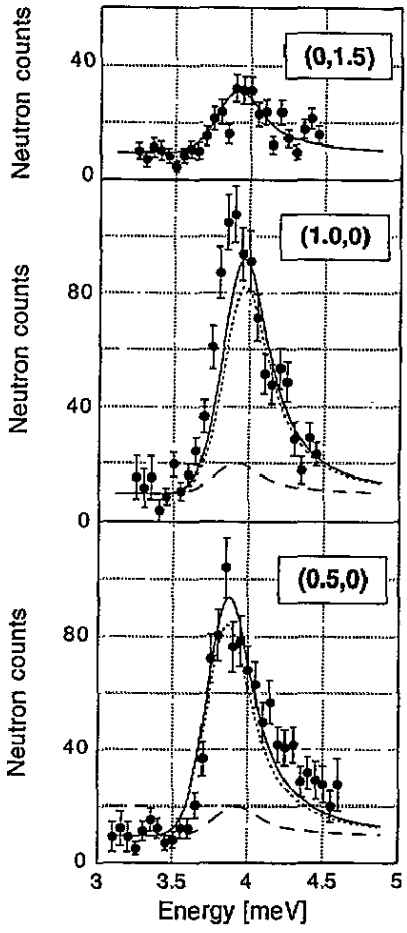

Figure 5. Normalized and form-factor-corrected energy spectra of neutrons scattered from grain-aligned $HoBa_2Cu_3O_7$ at 1.5 K for different scattering vectors Q. Here, the cooled beryllium filter was inserted between sample and analyser. The full lines correspond to the calculated excitation spectra as explained in text. The broken and dotted lines represent transverse and longitudinal polarizations, respectively.

much weaker than for $HoBa_2Cu_3O_7$ as actually expected from the larger CEF transition energy Δ (see (*4a*)). Because of the tetragonal symmetry some additional conditions are imposed on the magnetic coupling parameters and to the CEF dipole transition matrix elements: $J_a^{\perp} = J_b^{\perp} = J^{\perp}$ and $J_a^{\parallel} = J_b^{\parallel} = J^{\parallel}$, and $M_x^2 = M_y^2 = \frac{1}{2}M_{\perp}^2$. As for $HoBa_2Cu_3O_7$ we assumed $J_c^{\alpha} \approx 0$. Seventeen energy spectra were simultaneously fitted, and the refined parameters were an overall scale factor, the CEF transition energy Δ, the CEF dipole transition matrix elements $M_{\perp}$ and M_z with the condition $M_{\perp}^2 + M_z^2 = 32$ [12] and the magnetic coupling parameters $J^{\perp}$ and $J^{\parallel}$. The convoluted line shape function was determined as described in section 3.2. Again, a simplification to isotropic magnetic coupling is possible by setting $J^{\perp} = J^{\parallel} = J$. The results obtained for grain-aligned $HoBa_2Cu_3O_{6.2}$ are given in table 2. Here, the extension to anisotropic magnetic coupling does not considerably improve our fit. We noticed that the CEF transition energy Δ and the magnetic coupling parameter J are extremely correlated in the fitting procedure. It is therefore very hard to extract an

accurate magnetic coupling parameter J without a precise knowledge of the CEF transition energy Δ.

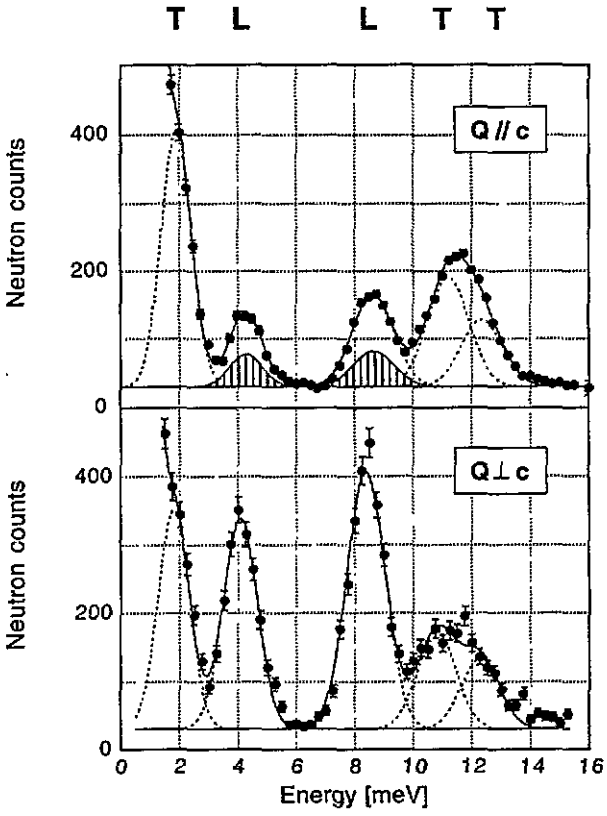

Figure 6. Energy spectra of neutrons scattered from grain-aligned $HoBa_2Cu_3O_7$ at $T = 1.5$ K with scattering vector Q parallel and perpendicular to the c axis ($Q = 1.72$ Å^{-1}). The measurements were performed with use of the triple-axis spectrometer IN2 installed at the reactor Saphir at PSI with constant analyser energy 14.95 meV. The lines denote Gaussian *fits to the observed* CEF *transitions. T and L refer to the dominant transverse and longitudinal* character of the CEF transitions. The shaded area corresponds to the transition strength due to the misorientation of the sample.

Recent measurements performed on $Y_{0.9}Ho_{0.1}Ba_2Cu_3O_{6.13}$ under high-energy resolution *conditions revealed a splitting of the lowest-lying* Γ_5 *doublet into two singlets* [18]. *The* splitting turned out to be about 0.1 meV and was explained in [18] as a result of the exchange interaction with the antiferromagnetically ordered subsystem of copper spins. In the present measurements we have not been able to resolve this splitting.

4. Discussion

In both the orthorhombic and tetragonal phases of grain- aligned $HoBa_2Cu_3O_x$ we have obtained fitted parameters Δ and M_α ($\alpha = x, y, z$) which are characteristic of the CEF interaction. The refined CEF transition energies Δ are found to be in good agreement with measurements performed on powders [11, 12]. Surprisingly, our fits always give non-vanishing CEF transition matrix elements M_α for all three Cartesian components $\alpha = x, y, z$.

This is in contradiction to the symmetry relations derived from the CEF interaction which require all the CEF transitions to have either longitudinal or transverse symmetry. More specifically, for $Q \parallel c$ we should not observe excitations associated with longitudinal polarization which follows directly from the polarization factor in the cross-section formula (3). For example, the longitudinal CEF ground state transition $\Gamma_3 \rightarrow \Gamma_1$ at 3.8 meV should be absent for $Q \parallel c$, however, this transition is present, although considerably reduced in intensity compared to the results for $Q \perp c$ (figures 5 and 6). The same effect occurs for another longitudinal CEF ground state transition at around 8 meV (figure 6). Similar arguments hold for the transverse CEF excitations which for $Q \parallel c$ are expected to be twice as intense compared to $Q \perp c$; however, the experimental data displayed in figure 6 are clearly at variance with the CEF-only model. Similarly, the CEF interaction in $HoBa_2Cu_3O_{6.2}$ predicts a purely transverse ($M_\perp \neq 0, M_z = 0$) CEF transition $\Gamma_3 \rightarrow \Gamma_5$ at $\Delta \approx 1.1$ meV [12], in contradiction to the results of our fits (see table 2).

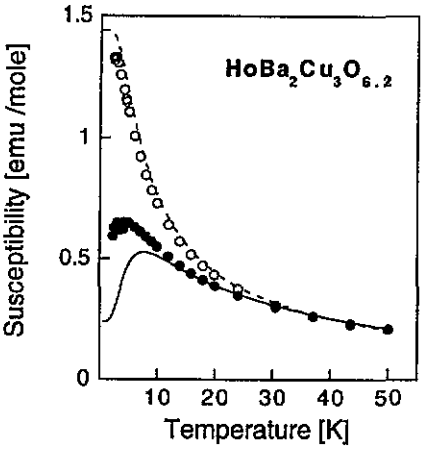

Figure 7. Temperature dependence of the magnetic susceptibility χ for grain-aligned $HoBa_2Cu_3O_{6.2}$. The full and empty circles correspond to the components $\chi^{\parallel}$ and $\chi^{\perp}$ parallel and perpendicular to the c axis, respectively. The lines are the result of calculations based on the CEF interaction.

There are several factors which may explain the above-mentioned discrepancies. The finite 'mosaic spread' of our samples leads to an effective spread of the scattering vector Q which is therefore never ideally parallel or perpendicular to the c axis. This effect is proportional to $\sin^2 \alpha$ ($\alpha = 11°$ is the HWHM of the measured rocking curve, see figure 1), and it amounts to a few per cent only. The unoriented fraction of our grain-aligned samples (which amounts to 15%, see section 2) also contributes to INS scattering but without distinction of the longitudinal or transverse character of CEF transitions. The scattering contributions due to both the finite mosaic spread and the unoriented fraction have been calculated based on the rocking curve displayed in figure 1 (lower part) and are shown as shaded areas in figure 6. These effects, however, are not strong enough to explain alone the observation of the longitudinal CEF transitions for $Q \parallel c$. Parts of the observed discrepancies are most likely due to exchange effects which mix the CEF wave functions in such a way that the CEF transitions lose their distinct (longitudinal or transverse) character. This explanation has been used to interpret similar discrepancies in INS experiments on a perfect single crystal of $PrNi_5$ [19].

A similar situation is encountered in the magnetic susceptibility data obtained for our

grain-aligned sample $HoBa_2Cu_3O_{6.2}$ with use of a SQUID magnetometer in an applied field of 500 Oe, which cannot be reproduced by the CEF model (see figure 7). The disagreement between measurement and CEF calculation is particularly pronounced for the longitudinal component $\chi^{\parallel}$ at low temperature, where the magnetic susceptibility is essentially governed by the lowest-lying CEF states.

5. Conclusions

By means of neutron spectroscopic investigations on grain- aligned samples we have been able to separate the magnetic interaction into all its components as well as to prove the essentially two-dimensional nature of the magnetic coupling between the Ho^{3+} ions in $HoBa_2Cu_3O_x$. The Ho spins in $HoBa_2Cu_3O_7$ turn out to be ferromagnetically and antiferromagnetically coupled along the *a* and *b* axes, respectively. This is in agreement with the long-range magnetic ordering of the Ho spins observed at low temperature [6]. The magnetic coupling becomes weaker when the oxygen content is reduced. The coupling of the Ho spins is presumably dominated by nearest-neighbour superexchange interactions mediated by the same oxygen ions as bridges which also take place in the superconducting processes.

Acknowledgments

Financial support by both the Swiss National Science Foundation and the Bundesamt für Bildung und Wissenschaft is gratefully acknowledged.

References

[1] Fischer P 1995 *Current Status and Future Directions in Condensed Matter Physics* ed S K Malik to be published
[2] Maletta H, Chattopadhyay T and Brown P J 1990 *Physica* C **166** 9
[3] Clinton T W, Lynn J W, Lee B W, Buchgeister M and Maple M B 1993 *J. Appl. Phys.* **73** 6320
[4] Alp E E, Soderholm L, Shenoy G K, Hinks D G, Capone D W II, Zhang K and Dunlap B D 1987 *Phys. Rev.* B **36** 8910
[5] Misra S K and Felsteiner J 1992 *Phys. Rev.* B **46** 11033
[6] Roessli B, Fischer P, Staub U, Zolliker M and Furrer A 1993 *Europhys. Lett.* **23** 511; 1994 *J. Appl. Phys* **75** 6337
[7] Chen Y Y, Lai C C, Chiou B S, Ho J C and Ku H C 1993 *Phys. Rev.* B **47** 12 178
[8] MacIsaac A B, Whitehead J P, De'Bell K and Sowmya Narayanan K 1992 *Phys. Rev.* B **46** 6387
[9] Yang K N, Ferreira J M, Lee B W, Maple M B, Li W H, Lynn J W and Erwin R W 1989 *Phys. Rev.* B **40** 10 963
[10] Staub U, Fauth F, Guillaume M, Mesot J, Furrer A, Dosanjh P and Zhou H 1993 *Europhys. Lett.* **21** 845
Staub U, Fauth F, Guillaume M, Mesot J, Furrer A, Dosanjh P, Zhou H and Vorderwisch P 1994 *J. Appl. Phys.* **75** 6334
[11] Furrer A, Brüesch P and Unternährer P 1989 *Phys. Rev.* B **38** 4616
[12] Allenspach P, Furrer A, Brüesch P, Marsolais R and Unternährer P 1989 *Physica* C **157** 58
[13] Fulde P 1979 *Handbook on the Physics and Chemistry of Rare Earths* vol 2, ed K A Gschneidner Jr and L Eyring (Amsterdam: North-Holland) p 293
[14] Jensen J and Mackintosh A R 1991 *Rare Earth Magnetism* (Oxford: Clarendon)
[15] Lovesey S W 1984 *Theory of Thermal Neutron Scattering* (Oxford: Clarendon)
[16] Hälg B and Furrer A 1986 *Phys. Rev.* B **34** 6258
[17] Guillaume M, Staub S, Fauth F, Mesot J, Furrer A and Carlile C J 1994 *Physica* C **223** 333
[18] Aristov D N, Maleyev S V, Guillaume M, Furrer A and Carlile C J 1994 *Z. Phys.* B **95** 291
[19] Amato A, Bührer W, Grayevsky A, Gygax F N, Furrer A, Kaplan N and Schenck A 1992 *Solid State Commun.* **82** 767